Plastic properties of gold surfaces nanopatterned by ion beam sputtering

Plastic properties of gold surfaces nanopatterned by ion beam sputtering

V Navarro[1]**, O Rodríguez de la Fuente, A Mascaraque and J M Rojo**

Departamento de Física de Materiales, Universidad Complutense de Madrid,
E-28040 Madrid, Spain

E-mail: violeta.navarro@fis.ucm.es

Abstract

We review the mechanical properties of defective roughened surfaces with the major emphasis on nanoindentation work. We also report novel results in which force versus penetration curves and AFM images of the nanoindented surface are compared for a flat surface of Au(001) and an Ar^+ bombarded one, both with a high and a low flux of ions. We have found that bombarded surfaces yield at a lower stress than untreated flat ones. Surfaces bombarded at high flux show a large roughness and their yield point, marking the onset of surface plasticity, decreases with respect to that of the flat surface or of the surface bombarded with a low flux. The present results are compared with earlier work on nanoindented vicinal surfaces in which the sole surface modifications with respect to the flat surface were the presence of a high density of steps. It is concluded that a softening effect due to the bombardment-induced nanostructure of the surface dominates over the hardening one due to defect creation and interaction in the surface neighbourhood.

(Some figures in this article are in colour only in the electronic version)

1. Introduction

In recent times, the role of surfaces in governing the mechanical properties of solids is being increasingly recognized. This role turns pre-eminent as the size of the sample falls into the nanometre range. In the now prevailing realm of nanostructures, the study of surface mechanical properties becomes, then, of paramount importance. A good example is provided by the present surge in the development of microelectromechanical devices (MEMS), a type of device in which a thorough characterization of their mechanical properties is mandatory. Most of our present understanding of those properties stems from studies in metals, most conspicuously in gold. Apart from being the metal which has been most thoroughly studied, gold is interesting from the point of view of applications. Good examples are its continuous utilization in electronic nanostructures or in the shape of catalyst nanoparticles [1, 2]. In recent times, nanoindentation has been developed as the technique of choice to characterize surface mechanical properties [3, 4]. The combination of experimental indentation work [5–9]— often carried out with the same tip which generates atomic

force microscopy (AFM) images—with molecular dynamics simulations has been especially fruitful.

Real surfaces are known to be rich in defects, either intrinsic or introduced by external manipulation. The role of pre-existing surface defects on surface mechanical properties is a particularly important—albeit little analysed—issue. Early studies [10, 11] have shown that a certain type of such defects—surface steps—soften the crystal in their vicinity and more recent research [12] has added support to that result from experiments on more realistic surfaces, having further disclosed mechanisms for the referred softening. Ion bombardment is known to create a very diversified set of surface point defects—either individual or clustered—dislocations and changes of microstructure patterns and one should be aware that all of those features can modify the surface mechanical properties.

Much experimental and theoretical research has been done during the last few years to investigate the basic atomistic processes behind the morphological evolution of the surface (for recent reviews see [13–15]). There has also been much work focused on the study on the physicochemical properties arising from the structural modification.

1

For example, reactive [16] and magnetic [17] properties have been investigated in surfaces previously modified by ion bombardment. However, nanomechanical properties of these ion-modified surfaces are probably one of the least studied set of properties. Although much has been learnt about the types of ion-induced surface modifications, particularly in gold [18], the present gaps in our knowledge of defect kinetics, interactions between point defects and dislocations and cooperative effects result in the absence of a clear map of surface and sub-surface defect distribution. In particular, much would be gained by knowing this distribution as a function of the external parameters, ion flux and substrate temperature. A shortage of information about this dependence hinders the possibility of establishing a clear pathway between surface structural modifications and surface mechanical properties.

In the present work, we report on new experimental and simulation results on the correlation between ion-bombardment modification of metal surfaces and surface mechanical properties in gold. To place these results in a more general framework, in section 2 we review, first, our present knowledge of surface mechanical properties, emphasizing the information that can be obtained from nanoindentation experiments. We also review the role of surface defects on those mechanical properties, with special attention to defects originated in ion-bombarded surfaces. In particular, we compare surface defects induced by bombardment with those introduced by alternative processes. After an overview in section 3 of the experimental methods and simulation procedures that we have used, we report in section 4 novel experimental results on the mechanical behaviour of ion-bombarded surfaces as compared to unbombarded ones. We also include comparative results from the simulation analysis in the different conditions. Specifically, nanoindentation penetration curves in both types of surfaces are contrasted. The implications of these results are fully discussed in section 5. We discuss bombardment effects in terms of a competition between two opposing factors, both of them arising from surface bombardment: a hardening factor originating in the sub-surface defect structure and a softening one originating from the surface step stepping and patterning. We close with a section 6 in which we summarize our present knowledge of the role of surface defects on mechanical properties.

2. Surface defects and mechanical properties: a review

2.1. Surface defects and nanopatterning with ion bombardment

There is now a considerable body of knowledge concerning the defect structure originated *in the bulk* as a consequence of particle irradiation, for example, following neutron or high energy (MeV) He^+ irradiation [19]. Less detailed information is available about irradiation involving ions in the low energy range, in which the role of surfaces becomes of paramount importance. On the other hand, low energy ion beam erosion is, undoubtedly, a valuable tool for nanostructuring surfaces. Usually, the surfaces are bombarded at saturation fluences

and, depending on the experimental parameters, such as temperature, ion flux, material properties, incidence angle of the beam, etc, a wide variety of different morphologies can be obtained. The physics lying behind these phenomena is based, basically, on self-organization processes taking place when two competing trends occur simultaneously: ion bombardment, which tends to damage the superficial region, and surface diffusion, which tends to anneal out the generated defects.

The impact of an ion against a solid with an energy of the order of 1 keV produces the ejection of atoms away from the material and a cascade of events in a shallow region below the surface. For fluences smaller than those corresponding to damage saturation, new types of defects are left behind after irradiation in both the surface and sub-surface region of the sample. While the recombination of the generated defects eliminates most of the damage, a few defects remain. The most prevailing ones are vacancies, interstitials and adatoms. Diffusion and atom sputtering finally favours the relative population of surface vacancies. In fact, the evolution of surface morphology during ion irradiation can be explained, under the simplest assumptions, in terms of the creation, diffusion and clustering of surface vacancies. Their aggregation form critical nuclei which usually evolve into larger vacancy islands and, then, to more complex structures [20–22]. However, we have shown in the past [18, 23, 24] that reconstructed surfaces show a wider variety of defects induced by ion bombardment. For example, in the case of the 5×1 hexagonal reconstruction of the (001) surfaces of fcc Au, Pt and Ir, the first generated defects resulting from the aggregation of individual vacancies are not vacancy islands but two-dimensional dislocations. They result both from the anisotropic character of surface diffusion and from the relative decoupling between the first and second surface atomic layers. Other surface defects associated with the reconstruction appearing after larger ion doses are orthogonal reconstruction domains and unreconstructed patches. After increasing the ion dose, multiple atomic levels are formed due to the clustering of new vacancy islands inside previously existing islands. An example of the different surface morphologies dependent on the ion dose is shown in figure 1 for an Au(001) surface.

If the ion flux is sufficiently high (its threshold value being temperature-dependent), competition between the two trends mentioned above takes place and a rough surface with a relative good lateral order, in the form of *ripples* or craters and mounds, may become apparent[2]. In the case of Au(001), we have shown that, under normal beam incidence, a quite well-ordered chequerboard pattern is recognized for high ion fluence and flux [26]. A similar pattern has been reported for Ag(001) [27].

It is worth noting that the extent of the structural damage is not limited to the upper layer. As is well known, after a sufficiently high temperature annealing of a rough surface, a flat surface is recovered. However, we have observed [6, 18, 28] that, if this annealing is not large or long enough, sub-surface interstitial loops are formed in the otherwise defect-free pristine terraces. In an Au(001) surface

---

[2] Other papers in the present issue of this journal are devoted to this nanopatterning.
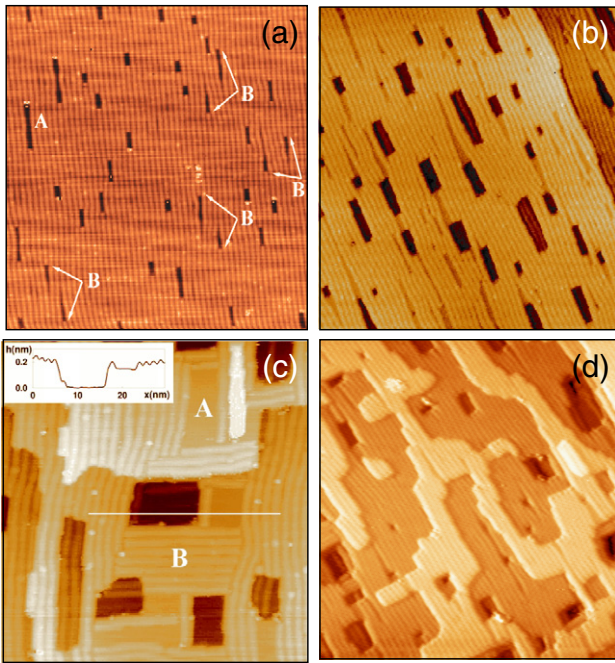
Figure 1. STM images of the Au(001) surface bombarded with increasing Ar$^+$ doses (doses measured in units of ML$^+$, equal to one ion per unreconstructed gold Au(001) surface). The doses are approximately, from (a)–(d): 0.05 ML$^+$, 0.25 ML$^+$, 0.5 ML$^+$ and 5 ML$^+$. The configuration of the defects are: (a) (83 × 83 nm^2) two-dimensional dislocation dipoles in the form of elongated defects and pairs of single two-dimensional dislocations, indicated by A and B in the figure. (b) (81 × 81 nm^2) vacancy islands and other kinds of defects stemming from them. (c) (45 × 45 nm^2) unreconstructed surface regions (A) and reconstruction domains rotated 90° with respect to the original direction. The inset shows a profile. (d) (86 × 86 nm^2) multiple atomic levels, as a result of the nucleation of vacancy islands inside previously existing vacancy islands. Reproduced with permission from [25].

these loops have the structural configuration of a truncated hillock (also called *mesa*). These loops are most likely originated by the diffusion and aggregation of sub-surface interstitials formed during ion irradiation. As we shall discuss later in the text, the existence of both surface and sub-surface defects in ion-bombarded surfaces must be considered for the study of nanomechanical properties of these modified surfaces.

2.2. Mechanical properties of surfaces

As every textbook recognizes, mechanical properties of solids are controlled by defects and, more specifically, by dislocations [29]. Solids yield at a much lower resolved shear stress, τ_c, than the one theoretically predicted for an ideal crystal because *pre-existing* dislocations initiate glide at these much lower stresses, resulting in an irreversible slip of compact planes on each other. Had these dislocations not been present in the crystal, the shear stresses necessary to trigger this slip process—usually called theoretical resolved shear stress, τ_{th}— would be of the order of $\tau_{th} \approx \mu/2\pi$, where μ designates the shear modulus of the crystal. Albeit, experimentally τ_c is orders of magnitude smaller than τ_{th}. Hardness, H, is another important mechanical property, if not the easiest one to define

accurately. It is supposed to be a property of the bulk, not of the surface of the material. Hardness has been traditionally measured by indentation tests. This is due to the fact that traditional indentations involves penetrations of the order of microns or more and are supposed to probe the bulk of the sample. Size effects at the nanoindentation level are beginning to be explored in nanostructures [30]. Bridging the gap between bulk-and surface-dependent mechanical properties has received comparatively little attention [31].

In the present work, we are interested in exploring the mechanical properties of ion-bombarded surfaces. As ion-bombardment damage is relatively shallow, it is unlikely that bulk-sensitive properties are much affected. Surface mechanical properties, in contrast, are expected to be modified. In order to specifically explore surface mechanical properties, nanoindentation has been developed [3, 4, 32] and we shall devote most of this section to reviewing the knowledge obtained therefrom. Nanoindentation does not simply involve a reduction of scale with respect to larger scale indentation (including microindentation) but activates new mechanisms which are not operating in the bulk [33]. Although the details are still open to discussion [34], a combination of experimental [35–40] and simulation [41–43] work discloses the following trends. Locally, around a nanoindentation, yield is controlled by dislocation-loop nucleation and the stress required to *nucleate* a dislocation loop is much higher than the one required to *move* pre-existing dislocations—as is the case in the bulk, probed by indentations in the micrometre range. In fact, the former resembles the value theoretically predicted for an ideal crystal, τ_{th}. This special behaviour of surfaces is due to the fact that the concentration of pre-existing dislocations in the *effective volume* around the nanoindentation contact point is practically free of defects [44]. One can naively state that surfaces have mechanical properties which are similar to those of an ideal (defect-free) solid.

In the present section, we shall discuss the information on mechanical properties of surfaces which has been gathered from earlier nanoindentation experiments. Most of the quantitative information about the deformation processes from nanoindentation experiments is obtained via penetration curves, in which external force (also called load), F, is recorded as a function of penetration, h. We shall compare the properties of nearly-perfect flat surfaces of those of real-crystal surfaces. Real crystals are not surrounded by ideal surfaces, i.e. surfaces that correspond to perfect low-index crystal planes. On the one hand, surfaces are seldom free of steps, isolated or in bunches, resulting from either small miscuts in the directions of cleavage or from the very process of lapping. Also, many types of other surface defects, e.g. surface vacancies, adatoms, vacancy islands, dislocations, etc, can be present either as a left-print of the processing of the material or from the *intentional* introduction of these defects by a number of different methods. Those due to ion irradiation have been described in section 2.1.

Along the penetration curve, one can distinguish two main stages of the deformation process: elastic and plastic. For each stage, we first review the current understanding of ideal (or quasi-ideal) surfaces and then turn to the discussion of surfaces with defects and/or nanopatterning.

2.2.1. Elastic region. At the beginning of a penetration curve, there is always an elastic stage. It is characterized by: (i) the penetration curves are fully reversible and (ii) upon retraction of the tip, there is no visible trace left in the surface. In microindentation tests, often a spherical indenter is used. This is not the case in nanoindentation where, most often, tips in the shape of pyramids or conical shapes are employed. However, for small penetrations—as is the case in the elastic region— practically any tip can be approximated by a spherical sector; we shall call R the radius of the corresponding sphere. As will be shown later, this approximation is in good agreement with the experimental data.

In terms of the theory of elasticity, a full analysis of the penetration curve of a spherical tip on a plane surface has been first performed by Hertz [45]. Although more recent models, such as the JKR [46] or DMT [47] models, have included adhesion terms in the tip–sample interaction, we have neglected them in our study. Except for the jump-to-contact and the pull-out forces, adhesion forces do not show up at the elastic part of the indentation curve and this often shows a good Hertzian behaviour. At the nanometric scale (with forces well below 1 μN), the literature shows that, whenever the elastic ranges of the nanoindentation curves have been fitted to a model, this has been the Hertz model most of the times. Furthermore, as we will show in section 3.1, we have used a diamond tip to reduce adhesion effects.

Hertz, in his model, showed that the force, F, and penetration, h, are related by

$$F = \tfrac{4}{3} R^{1/2} E^* h^{3/2} \tag{1}$$

where E^* is the reduced Young modulus, given by

$$\frac{1}{E^*} = \frac{1 - \nu^2}{E} + \frac{1 - \nu'^2}{E'} \tag{2}$$

where the primes denote the elastic parameters of the tip. One uses the reduced modulus E^* to account for the deformation of the tip itself. It can be shown that one can work the theory as if the tip were infinitely hard on condition that equation (2) is substituted for the Young modulus of the sample.

The geometry of the contact is shown in figure 2. From simple geometry, the radius of the contact circle between tip and sample, a, can be written in terms of h_c, the distance from that circle to the maximum penetration depth:

$$a^2 = R^2 - (R - h_c)^2 = 2Rh_c - h_c^2 \tag{3}$$

which, for small penetrations, $h_c/2 \ll R$, characteristic of the elastic stage, reduces to

$$a^2 = R^2 - (R - h_c)^2 = 2Rh_c. \tag{4}$$

A most important result of Hertz's analysis is that the contact circle is situated at the *half-depth* of the maximum penetration, h [45]. Consequently, $h_c = h_z = h/2$ and one can write

$$a^2 = Rh. \tag{5}$$

The strength of the nanoindentation is characterized by a mean contact pressure (MCP), $\bar{p}$, defined as the external force
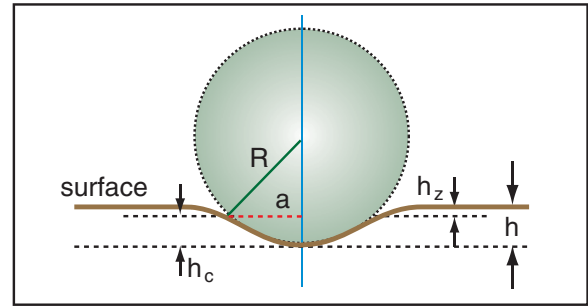

Figure 2. Geometry and basic parameters in spherical indentation.

divided by the area of the contact circle. In terms of the penetration, one can write

$$\bar{p} = \frac{F}{\pi Rh}. \tag{6}$$

The value of the Young modulus, E, which is obtained by fitting the experimental data to equation (1) and, further, using equation (2), gauges the *stiffness* of the material. From the physical point of view, it is worth noting that E is directly related to the bonding of the atoms. Contrary to other mechanical properties, such as the yield strength, stiffness is relatively insensitive to the previous treatments of the sample.

Although much effort has been devoted to understanding the variations of elastic moduli following ion irradiation in insulators and semiconductor thin films, metallic surfaces have not conveyed much interest. As we mentioned above, elastic moduli depend basically on the bonding of each atom to its neighbours and, in the case of insulators, bond-breaking following ion irradiation is expected to be very efficient. However, in the case of metals, electron screening would tend to reduce bombardment effects and the high mobilities (at room temperature) of point defects would also minimize the contribution of bond-breaking to the elastic moduli.

In some cases, the values of E^* obtained from nanoindentation experiments by using equation (1) are seen to decrease upon surface irradiation [12]. Note that in those experiments the surface acquires a nanostructured pattern, equivalent to a high density of steps, resulting in many surface atoms with a distorted environment. Consequently, intrinsic changes in E would not have been entirely unexpected. However, care has to be taken in the interpretation of the data as the measured value of E^* can be affected by external elements; for example, the formation of surface steps might considerably reduce the area of contact, leading to a real value of p higher than the corresponding one on the flat surface. This would result in an underestimation of E^*. On the whole, although there are hints, one cannot conclude that there is convincing evidence of a variation of the stiffness in irradiated surfaces.

2.2.2. Plastic region: flat surfaces. The transition from an elastic to a plastic regime is marked by the appearance of a series of discontinuities [37] in the penetration curve, which are usually named 'pop-ins' [48, 49]. In figure 3 we show an example of our recent work in Au(111) where the
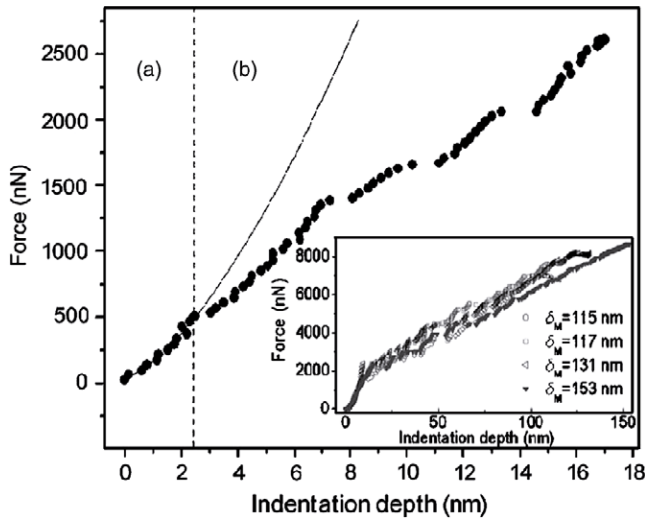
Figure 3. Discontinuities ('pop-ins') in the nanoindentation curve of Au(111) at the onset of plasticity. Inset: penetration curve in the plastic region. Note that the slope (a measurement of hardness) is practically constant. Reproduced with permission from [8]. Copyright 2006 by the American Physical Society.

appearance of those pop-ins has been unequivocally associated to dislocation generation around the nanoindentation point. Permanent traces visible by AFM are also left behind upon tip retraction. While the appearance of the pop-ins can be directly related to dislocation processes, the reciprocal is not necessary true [50, 51].

Nanoindentation allows us to explore a very small effective volume around the nanoindentation where surface properties are effectively probed. The yield point marks the transition from the elastic to plastic regimes. The corresponding MCP, $\bar{p}_Y$ can be obtained from the penetration curve by using equation (6), leading to

$$\bar{p}_Y \approx \frac{F}{\pi R h_Y}. \qquad (7)$$

The experiments show that the surface yields at a value of the mean contact pressure similar to the one expected from an ideal crystal. There are a number of examples in different metallic surfaces, namely in gold [8, 10, 37] or aluminium [52]. In figure 3 we show an example from our work in Au(111) [8]. There, by using equation (7), one obtains, for Au, a value of 2.5 GPa $< \bar{p}_Y < 6$ GPa, which indeed is comparable to the ideal crystal value $\mu/2\pi$. Simulations carried out by us and other groups confirm that *homogeneous* nucleation of dislocations take place below the terraces precisely when the maximum shear stress reaches the region of values corresponding to the critical resolved shear strength of an *ideal* crystal. This viewpoint is consistent with the measurements of Kiely and Houston [37] on the value of $\bar{p}_Y$ as a function of surface normal orientation in Au. Although they obtained different values of $\bar{p}_Y$ for the three main orientations, the projected maximum shear stress was found to be the same within experimental error.

Insight into the mechanisms involved in the different stages of the penetration curves is much reinforced when

AFM images corresponding to these stages are brought into comparison. Our systematic studies using both scanning tunnel microscopy (STM) and AFM have shown that there are different types of dislocation configurations which are generated following surface nanoindentation. We have discussed their morphology and dislocation fundamental in previous publications [53] and shall not go into them in detail here. A particular type of defect is worth remarking though: dislocation loops with *some* of their sides in a screw orientation (called 'screw-loops'). Once they are generated, these screw-loops can glide and cross-slip, resulting in the creation of surface steps that can be used as landmarks of their kinetics. An example of these processes is shown as figure 4. Note that not all the dislocations loops generated by the nanoindentation are visible by these techniques. Loops that, after being generated, glide into the bulk do not leave that kind of steps behind although they may certainly contribute to the concave traces remaining in the surface after tip retraction.

2.2.3. Plastic region: surfaces with defects. There is a wide variety of surface defects, either intrinsically generated in the course of sample preparation or deliberately inserted following specific treatments. The simplest ones are, perhaps, surface steps. There are well-established procedures to create them, even in ordered arrays, and their characterization is easier than that of point defects.

When surfaces are cut with a slight miscut angle with respect to a compact plane normal, the system relaxes to a periodic array of steps. These arrays can be identified either by the split of their LEED spots or by direct imaging with STM (or, at times, with AFM). LEED data also indicate long-range order and homogeneity of the surface. This is a adequate model system for a real surface, which commonly consists of more or less wide terraces separated by (often monoatomic) steps, the latter frequently clustering in bunches. Therefore, steps tend to be ubiquitous in all surfaces.

Steps are expected to locally modify plastic behaviour. In particular, the nucleation of a dislocation loop near a step might be expected to require a smaller energy than on the centre of a wide terrace. Experiments carried out with different configurations involving steps have confirmed those expectations. On an Au surface, Corcoran *et al* [10] found that, at the onset of the plastic region, the penetration curve near a bunch of steps ran below (softer surface) the corresponding one at the centre of a terrace. These results were confirmed by Kiely *et al* [54], which carried out the same type of measurement on a terrace near to and far from a *single* step. They measured a yield about 35–45% lower near the single step. They also found that the extension of the influence zone of the step far exceeded the diameter of the contact circle of surface and tip. Some of these results were reinforced by atomistic simulations [11], in which dislocations were *seen* to nucleate at lower stresses near the step. Whereas the critical resolved shear at the terrace was found to be of the order of the theoretical shear strength of the material, the value at which loops nucleated in the neighbourhood of the step was found to be about 40% lower.
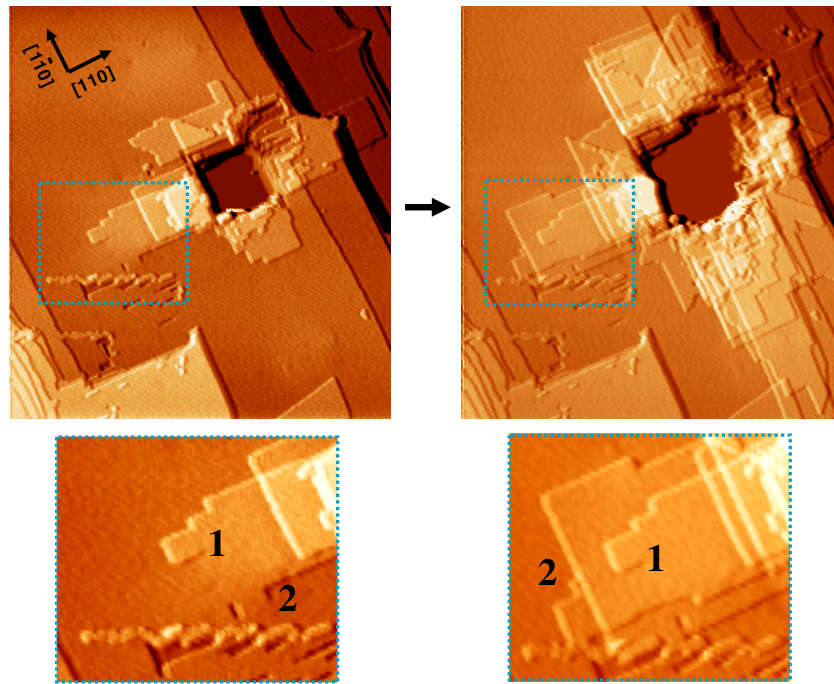
Figure 4. STM images of two successive nanoindentations superimposed on the same point of an Au(001) surface (the two frames below are magnified images). One can see (1) a screw dislocation which stays immobile after the second nanoindentation whereas a second screw dislocation (2) cross-slips in different {111} planes. Both the one-interatomic-distance high terrace steps and the superposition of terraces act as landmarks of the process. The scale of the top images is (530 × 530 nm²). Reproduced with permission from [53]. Copyright 2003 by the American Physical Society.
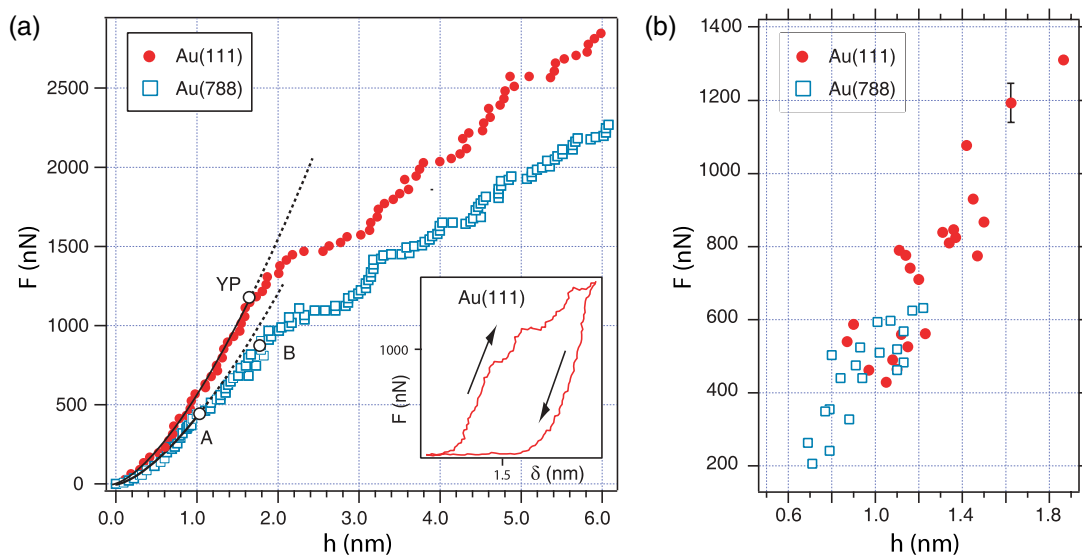

Figure 5. (a) Force, F, versus penetration, h, nanoindentation curves on flat (circles) and stepped (squares) Au surfaces; (b) statistics of yield stress values in both surfaces. Inset: indentation curve followed by retraction. Reproduced with permission from [12]. Copyright 2008 by the American Physical Society.

To create an environment more akin to real surfaces, we compared a flat Au(111) surface with a neighbouring Au(788) vicinal surface, in which a periodic range of steps covers the whole surface [12]. For either orientation, we carried out force versus penetration curves, at different maximum loads, and analysed the resulting surface damage by AFM. At the same time, we carried out atomistic simulations in order to visualize, at the atomic level, the processes taking place during dislocation nucleation and motion. The main results can be summarized as follows: (1) after a plastic, reversible, stage in which both surfaces follow a Hertzian model, the vicinal (stepped) surface yields—departs from a Hertzian curve—at a smaller load, $\bar{p}_Y$, than the flat one (see figure 5). (2) The flat surface transits directly between the elastic and plastic stages at $\bar{p}_Y$, the transit being marked by the generation of a series of pop-ins. The stepped surface has a different response: along a

region which we named the *intermediate* stage, the penetration curve gradually bends down, deviating continuously from the Hertzian shape, with no detectable pop-in. The parallel simulations carried out show that this behaviour arises from preferential dislocation nucleation beneath the surface steps. Progressing in the load, one ends up in the fully plastic stage, with ordinary pop-ins appearing in the penetration curve. (3) When the tip is withdrawn at a point in the intermediate state—before the full plastic state is reached—most of the dislocation loops generated beneath the surface steps retract and vanish, leaving behind a perfect crystal.

Three main conclusions can be drawn: (a) surface steps act as dislocation-loop nucleation sites with low activation energy, providing a clear example of heterogeneous defect nucleation under mechanical stress, (b) there is substantial dislocation activity prior to the appearance of pop-ins in the penetration curves and (c) contrary to common belief, a considerable fraction of the dislocations generated by the nanoindentation is unstable, being in equilibrium only in the presence of the indenting tip.

The above results are relevant to the subject of the present report because bombarded surfaces are rich in surface and sub-surface defects. In particular, surface steps arising from the interaction of ion-induced surface point defects are conspicuous, either in an ordered or in a disordered state. These steps are expected to co-exist with other types of surface and sub-surface defects also induced by the bombardment and the results shown hereafter aim at discriminating those contributions.

It is, then, expected that bombarded surfaces can have a different response to nanoindentation than normal-perfect ones. The experiments discussed for the first time in sections 4 and 5 of the present paper aim at analysing that different behaviour.

3. Experimental and computational details

3.1. Experimental details

Indentations are usually performed by applying a perpendicular force onto a surface with an appropriate tip (indenter). The relative geometry of tip and sample in a surface with defects is shown in figure 6. In order to quantify the mechanical properties of the solid under analysis, the mechanical properties of the indenter and its geometry must be known beforehand. Traditionally, macro- and microindentation tests have been performed with relatively large tips and mechanical actuators, whereas, more recently, indentation with nanoindenters or atomic force microscopes (AFM) have allowed indentations at the nanometric range. In this case, the size of the indentations is of the order of nanometres, while the size of the applied forces may be as small as tens of nanonewtons. Since the mechanical properties of a material, such as its hardness or Young modulus, may depend on the length scale, in some cases they need to be specifically determined for the nanoscale. A suitable tool for performing nanoindentations is the AFM, using the tip as the indenter although one should be aware that care has to be given to a number of checkings and corrections [55].
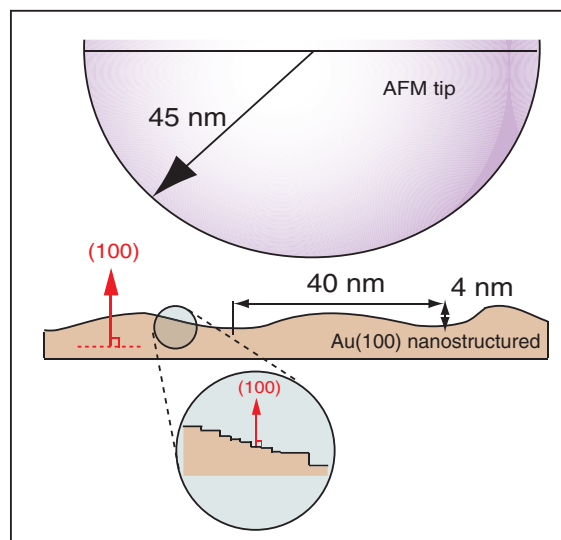

Figure 6. Geometry and basic parameters of the indentation on ion-bombarded surfaces. See details in the text.

AFM data have been treated with WSxM software [56]. The radius of the AFM tip is of the order of tens of nanometres and in special cases even smaller. In most cases, the same tip used for indenting can also be used to image the surface before and after performing the indentations. By analysing the modification of the surface after having performed the indentations, we can get a qualitative and quantitative idea of the mechanisms governing the deformation of the material [57].

When indenting with the AFM, the tip is placed on a specific point of interest over the sample located in the AFM image mode. To switch to the indentation mode, the feedback that controls the oscillation of the tip, or the deflection of the cantilever, is switched off as well as the cantilever oscillation in the case of the amplitude modulation mode. As the piezoelectric moves the sample towards the tip, the latter penetrates into the sample. The cantilever supporting the tip can be modelled as a spring which obeys Hooke's law with a spring constant k, characteristic of the cantilever and usually supplied by the manufacturer. In order to obtain an F versus h curve, the voltage, V, of the photodiode is measured as a function of the displacement of the piezoelectric Δ. Figure 7 shows an example of this data for a diamond tip penetrating in an Au(001) flat surface, with the loading and unloading sections. Adhesion effects are negligible compared to the indenter force as deduced from the absence of clear jump-to-contact or pull-out forces. To account for the cantilever deformation, a second penetration curve using a reference diamond surface is used. When pushing against this reference surface, the piezoelectric displacement Δ' is assumed to be due only to the cantilever deflection. For every value of the deflection voltage, the force, F, is then obtained as $F = k\Delta'$ and the effective penetration $h = \Delta - \Delta'$. The choice of the origin of force is the most conspicuous source of error. The origin of the curve is chosen when tip and surface sample are far away, so they do not interact. One would not expect, then, any deflection of the cantilever. However, the attractive component of the tip–sample interaction and related adhesion phenomena complicate the selection.
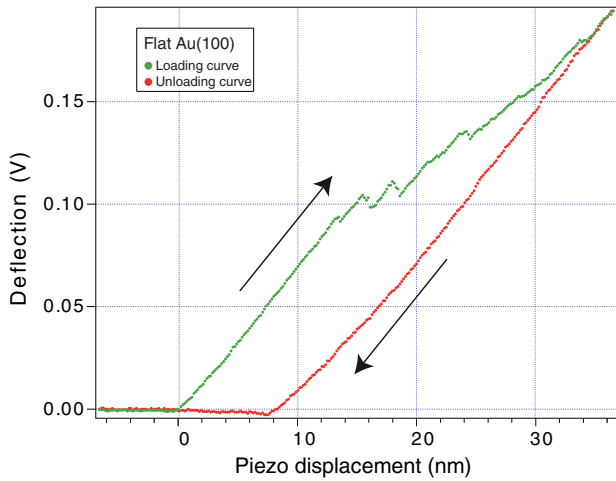
Figure 7. Photodiode voltage as a function of piezodisplacement for an Au(001) surface being indented by a diamond tip, with loading and unloading sections.

The tip and cantilevers used for indenting need to be carefully chosen depending on the material under study. There are two factors to take into account: the material from which the tip is fabricated and the stiffness of the cantilever. The tip's material should have both a Young modulus and a hardness much higher than that of the material under study; otherwise most of the deformation would take place in the tip, leading to unacceptable errors. Also the cantilever has to be stiff enough to let the tip penetrate inside the solid without excessive spring deformation. We have used silicon and diamond tips. The former, because of the spring constant and small radius, have the advantage of resolving the surface topography and the generated defects better. But quantitative results, such as those shown in figure 5, from which the yield stresses are determined, have all been obtained with the diamond tip. This reduces possible artifacts related to tip deformation and adhesion. The spring constant for the diamond tip is $k = 223$ N m^{-1}, as measured by the manufacturer individually for each tip. All AFM experiments have been carried out in ambient conditions.

To carry out the ion bombardment in UHV conditions, an Ar$^+$ ion beam is generated with a differentially pumped ion gun, its direction being normal to the surface. The sample is then transferred outside the chamber to perform the mechanical tests. To ensure a uniform dose in a square area of the sample with a side of a few millimetres, the beam is scanned in two perpendicular directions. The beam current density is measured with a Faraday cage. Because of the beam rastering, the ion current at a given point in the surface is not constant. The values for the fluxes appearing in the present work refer to the average value during a complete scan. In the present work we refer to a *high* flux ($\Phi = 4 \times 10^{13}$ ions cm^{-2} s^{-1}) and to a *low* flux ($\Phi = 2 \times 10^{12}$ ions cm^{-2} s^{-1}). We usually measure the fluences, θ^+, in units of ML$^+$, where ML$^+ = 1$ stands for a fluence of one incident atom per surface atom on the Au unreconstructed surface (1 ML equals 1.20×10^{15} atoms cm^{-2}). In all bombardment experiments, the fluences were high enough to ensure that sub-surface defect

saturation had been reached. For both high and low ion fluxes, the fluences exceeded $\theta^+ > 30$ ML$^+$.

3.2. Computational details

The simulations carried out in the present work are atomistic. The interatomic potential used is the embedded atom method for Au [58], which belongs to a wide and extensively used class of potentials, suitable for metallic systems. Computational atomistic simulations using this interatomic potential have already been carried out in our group to simulate surface plastic deformation in flat [18] and defective [12] surfaces, having shown a close agreement with the experimental measurements carried out in parallel.

Simulation cells, with lateral periodic boundary conditions and (001) top surface orientations, contain up to a few million atoms, depending on the specific simulation. The bottom layer is kept rigid, so that the whole system is not displaced downwards during indentation. Cell lateral dimensions are continuously scaled to keep the diagonal lateral components σ_{xx} and σ_{yy} of the stress tensor equal to zero. The nanoindenter is simulated as a spherical purely repulsive potential, thus ignoring all possible attractive and adhesion forces during approach and contact. The indenter radius varies between 40 and 100 Å. In every indentation step the nanoindenter position is lowered in steps of 0.01 or 0.02 Å. The whole system is then fully relaxed in this new configuration with a conjugate gradient minimization algorithm until system energy is minimized.

Sub-surface defects, in particular interstitials, are introduced in the simulation cell by randomly choosing their x and y coordinates and by generating a Gaussian distribution in z, centred around $z_0 = -10$ Å. Interstitials are initially placed in octahedral sites. Then a mild annealing at 300 K is applied during a few picoseconds to relax the structure. To visualize the simulated system the software AtomEye [59] is used.

4. Mechanical properties of ion-bombarded surfaces: experimental results

We have compared the response to nanoindentation, and in particular the onset of plasticity, in three types of Au(001) surfaces: flat (untreated) and bombarded with a high or low flux (numerical values above). We have measured by AFM the surface roughness after ion bombardment at saturation; comparative images are shown in figure 8. The differences between the two levels of flux are obvious. Measuring the surface roughness, σ by the peak-to-peak amplitude of the maximum vertical atomic displacement, for surfaces bombarded at high flux the surface roughness is $\sigma = 4 \pm 1$ nm. This roughness is one order of magnitude smaller after bombardment at low flux, about $\sigma = 0.4 \pm 0.1$ nm.

Nanoindentation F versus h curves have been obtained on the three types of surfaces. Results for mechanical parameters such as yield stress are known to exhibit a broad scattering. In part, this is due to the inhomogeneities of the surface but, also, to the intrinsic stochastic nature of the indentations [39]. To minimize the errors and to check reproducibility, we have
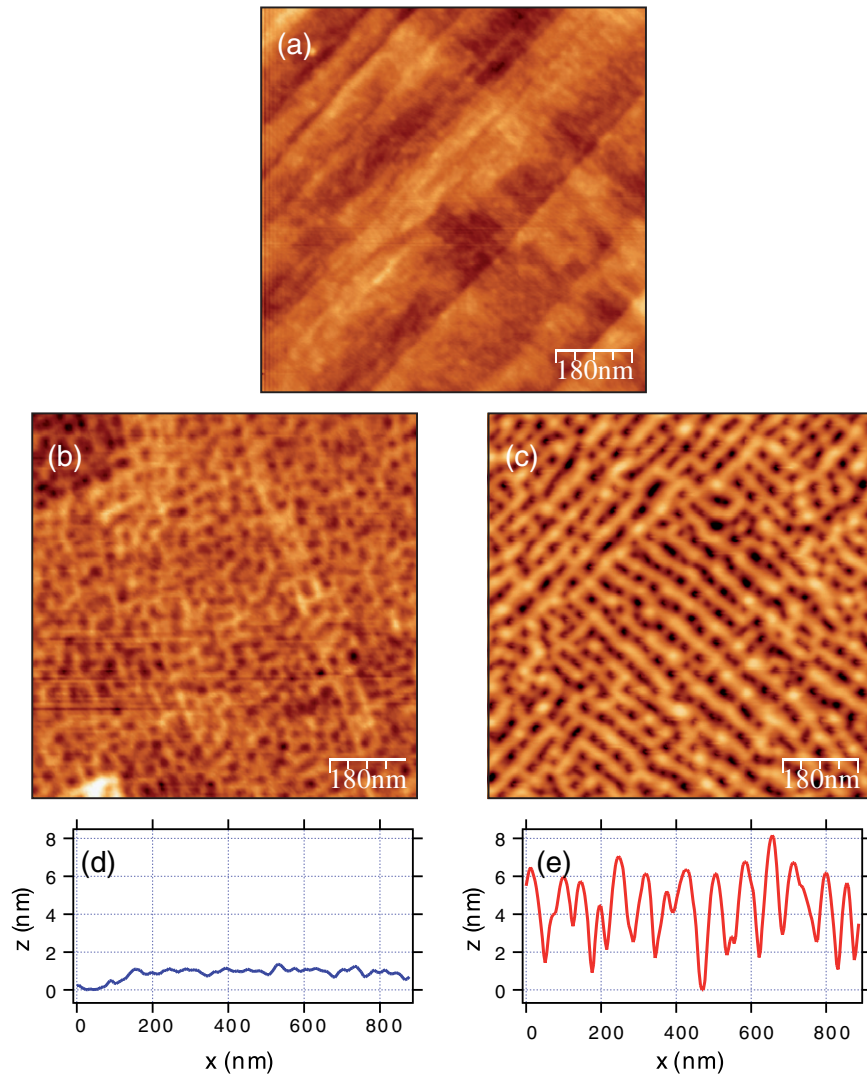
Figure 8. AFM images of (a) a flat Au(001) surface, (b) the same surface bombarded at saturation with low flux and (c) high flux of Ar$^+$. Quantitative scans of surface profiles along the dotted lines are shown as (d) for the low flux and (e) for the high flux. In each case, height (z) versus horizontal (x) coordinate are shown. Note that the roughness of (c) is an order of magnitude larger than that of (b).

usually carried out matrices of indentations. An example is shown in figure 9 in which nine nanoindentations with the same nominal maximum penetration are shown. Note the excellent reproducibility of the permanent traces left behind upon tip retrieval.

An example of the AFM images after indentation with a matrix involving successively increasing maximum penetration depths is shown in figure 10. The corresponding penetration curves for some of the matrix indentations are shown on its right-hand side. It is worth remarking that, below a certain threshold, no permanent trace is left behind after retrieval and this coincides with the absence of pop-ins in the penetration curves. The correlation between the appearance of pop-ins and the existence of permanent traces is patent.

It is worth remarking that piled-up material and terraces formed after indentation follow the preferential directions corresponding to the most compact atom rows ⟨110⟩. This is evidence that re-location of material is due to the movement and gliding of dislocations [26, 60, 61]. Notice also that, for

not too large penetrations, the rearrangement of the dislodged material around the indentation is controlled by the geometry of the atomic arrangement at the (100) surface.

The first stage of the force versus penetration curves corresponding to indentations for all three materials follows a Hertzian behaviour. The point at which these curves deviate from the Hertz model is taken as the yield point. In figure 11 we compare the penetration curve on a flat surface with the corresponding curve on a surface bombarded with a high flux. Note the significant descent in the yield stress of the latter. More quantitatively, the yield points of many indentations on the flat and modified surfaces are plotted in the same figure as a F_Y versus h_Y diagram. Although the scattering is significant, some trends emerge. Bombardment of the surface at high flux reduces the yield point of the surface with respect to the flat one whereas there is, at most, a slight change when the surface is bombarded at low flux. Comparing with the AFM images, one concludes that there is a significant correlation between surface roughness and decrease of the surface yield stress.
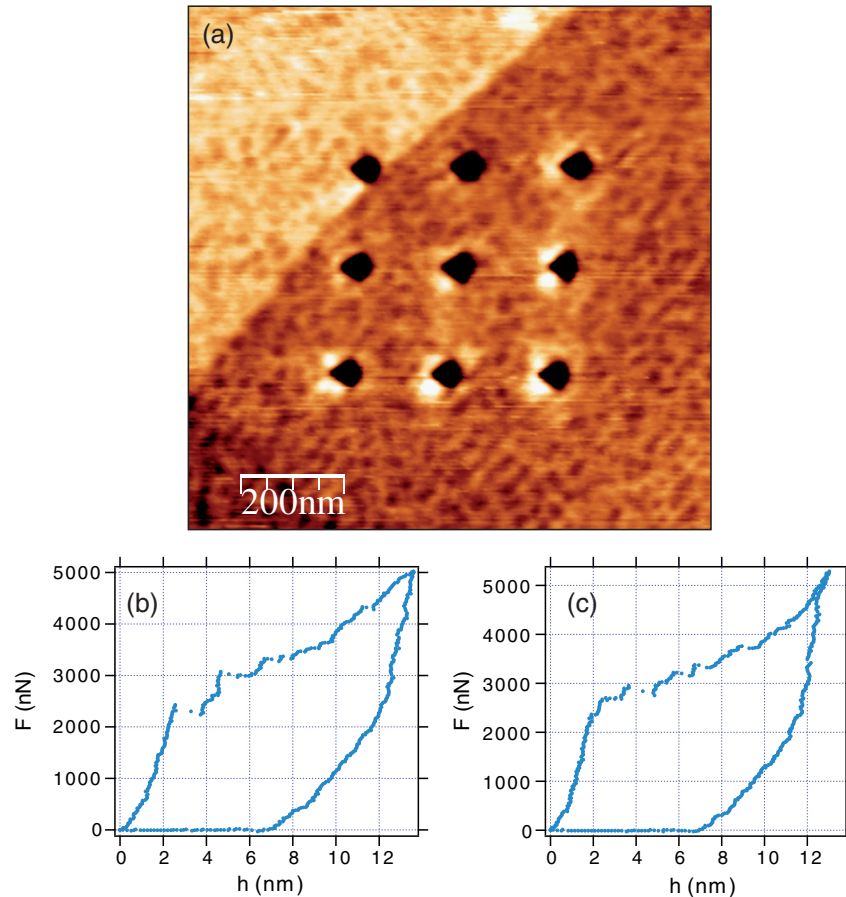
Figure 9. (a) AFM image of nine indentations performed at the same maximum applied load with a diamond tip on Au(100) surface sputtered at low flux, (b) and (c) force versus distance curves for loading and unloading of two of the indentations. These show the excellent reproducibility on both the traces left and also on the force–distance curves.

A large scattering of the data is characteristic of this kind of experiment, partly due to the intrinsic stochastic character of the yielding process [39].

5. Mechanical properties of ion-bombarded surfaces: analysis and discussion

In order to analyse surface mechanical properties, we propose the existence of two main competing mechanisms in ion-bombarded surfaces. Each mechanism is associated with a kind of structural defect, either at the surface or below it. The ion-induced roughness is, at the atomic level, constituted by many surface steps along the two equivalent directions, arranged to form a network of nanometric mounds and pits. We have already argued that stepped vicinal surfaces tend to lower the yield stress, but one must keep in mind that in vicinal surfaces all steps are equivalent [12]. The consequence is that the most incipient half-loops are nucleated in the same slip plane, leaving little chance for dislocations to interact. In contrast, for the case of ion-modified surfaces, all four types of steps co-exist: two (one ascending and one descending) for each ⟨110⟩ direction. No specific slip plane is thus preferred and all are active in a spatial range of a few nanometres. This, in principle, allows that half-loops nucleated along different slip planes may

intersect below the surface and form locks [62, 63]. Thus, a mechanical softening behaviour of rough surfaces, as has been shown in the case of stepped ones, cannot be ascertained *a priori*.

The other contribution to the mechanical response comes from sub-surface defects such as interstitials and vacancies. The interaction of point defects with dislocations is one of the most studied topics in the field of mechanical properties of materials [64].   Apart from the equilibrium spatial distribution of point defects around dislocations, based on elastic and thermodynamic criteria, their mutual interaction also affects dislocation motion. In general, point defects tend to lock dislocations through different mechanisms [65] and, consequently, augment the hardness of the solid. This idea is behind many of the technical processes aimed at hardening materials.

Our experimental results, displayed in figure 11, show a decrease of the yield point in ion-bombarded surfaces at high flux. To gain insight into the balance between the two competing mechanisms in ion-bombarded surfaces, we have performed atomistic simulations of nanoindentation processes under two different conditions. Here we report on simple but realistic cases which help to understand the observed trends and which may contribute to the bridging of the gap between model and real surfaces. In the first group of calculations, we
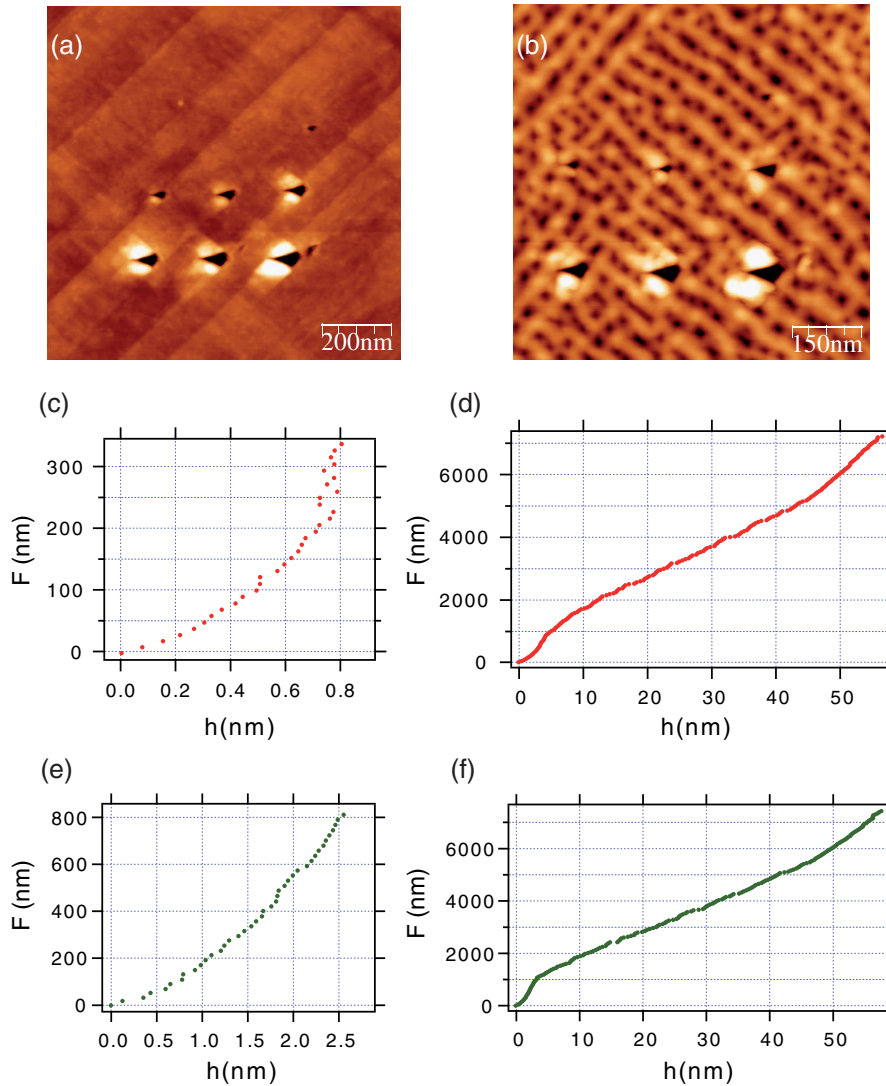
Figure 10. (a) and (b) show AFM images of indentations performed with a silicon tip with increasing maximum applied load on (a) Au(100) flat surface and (b) bombarded at high flux. Piled-up material around the indentations follows the two preferential directions ⟨110⟩ characteristic of this surface. This indicates a gliding mechanism of the dislocations formed upon indenting for the propagation of the dislodged material. (c) and (e) show force versus distance curves within the elastic regime for indentations at the lowest load. These indentations do not leave traces on the surface. (d) and (f) show force versus distance curves at the highest applied load where the two regimes, elastic and plastic, can be observed.

have simulated the surface roughness with model protrusions in the form of stepped pyramids (see figure 12). In the second group, we have modelled the role of sub-surface defects by introducing vacancies and interstitials below an initially flat and structurally perfect surface. Three different pyramids with different inter-step separation have been indented. The inter-step distance is constant for every pyramid, governing also its constant slope. In this way we simulate protrusions or asperities with different slopes defined by their faces, i.e. with different local roughnesses. During the indentation simulations, the indenter has initiated the mechanical contact directly onto the centre of the pyramid, which is first elastically and then plastically deformed. Figure 13 shows the simulated indentation *F*–*h* curves for the four cases. If we define surface hardness as being proportional to the force required to penetrate a given depth, we can conclude from figure 13 that a

protrusion always shows a reduced hardness compared to a flat surface. Moreover, the more stepped the pyramid is (the shorter their inter-step distance is), the softer it is. In this respect pyramids show, qualitatively, a similar mechanical response to stepped surfaces [12]. No dislocation interaction, eventually leading to local hardening, seems to show up. Dislocation kinetics, monitored with the snapshots during the simulation, show the interaction of the loops nucleated in all four different slip planes, but they do not seem to form stable locks under the applied pressure of the indenter. These results extend the general idea of a reduced hardness in stepped surfaces to the case of nanostructures such as the pyramids under study.

To simulate nanoindentation on surfaces with previous sub-surface point defects, we use a simplifying model involving either single vacancies or single interstitials. We have already referred to the difficulties in knowing the exact
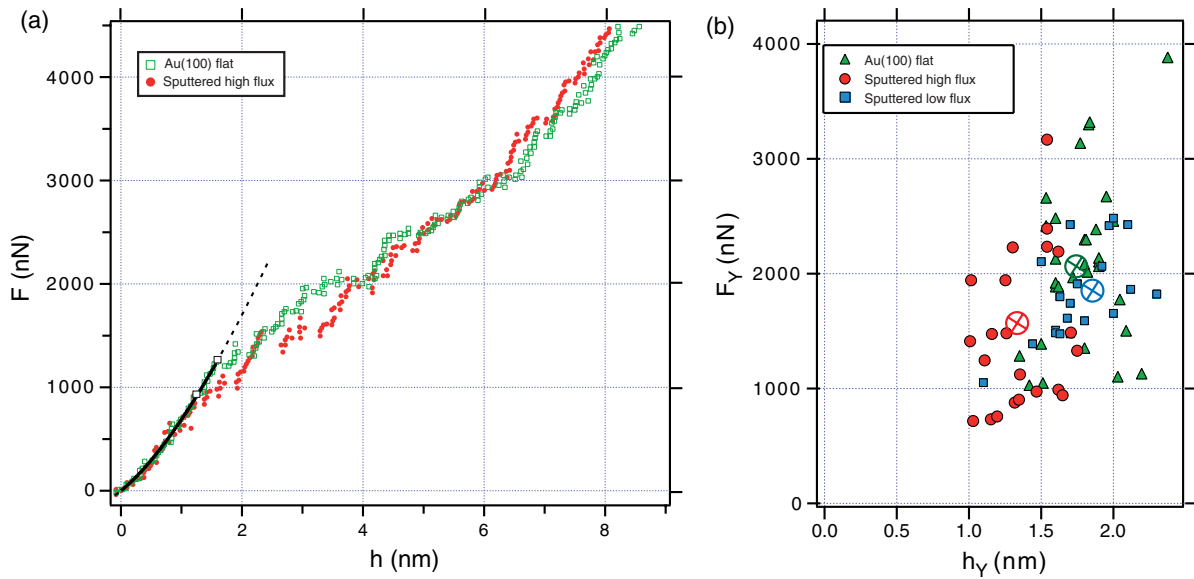
Figure 11. Comparison of force versus penetration curves for flat (open green circles) and sputtered (closed red circles) at high flux Au(100). Elastic regime for both fits well to a Hertzian behaviour (dashed black line), which terminates at the yield point for each surface. (b) Distribution of the yield points for various curves corresponding to the flat (green triangles), sputtered at high flux (red circles) and low flux (blue squares). The cross (x) inside a circle represents the mean value for each of them.
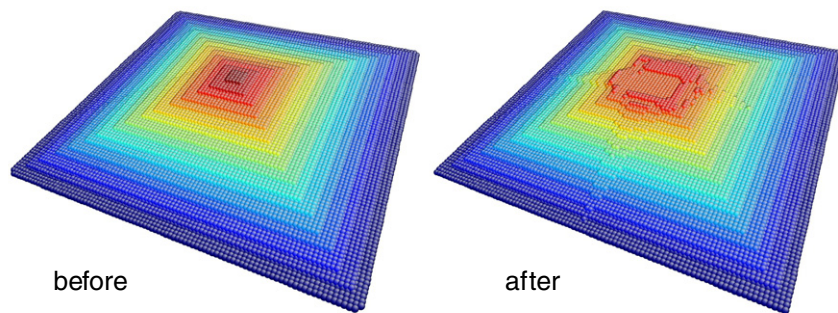

Figure 12. Example of a simulated pyramid, before (left) and after being indented (right). The top atomic levels are squashed by the indenter and traces of plastic deformation are visible in the faces.

configuration of sub-surface defects. In any case, the presence of interstitials after irradiation is demonstrated by the fact that we have observed, after mild annealing, surface defects of the *mesa* type [6, 18]. These type of defects derive from interstitial half-loops whose nucleation requires diffusion and clustering of individual interstitials. The initial interstitial disc forms a dislocation half-loop, which subsequently gives rise to the *mesa*. The number of interstitials in the latter is of the order of $\approx 10^3$.

In the present simulations, interstitials are observed to split in a *dumbbell* configuration during the simulated annealing. In this arrangement, the extra volume of the interstitial is shared by two atoms along a $\langle 110 \rangle$ direction. In other words, two equivalent atoms share one regular lattice site. The *dumbbell* is a frequent configuration known to take place in fcc metals. The indentation curves indicate a surface hardening behaviour. They reflect a slightly increasing hardness for the surfaces with self-interstitials and vacancies, with respect to flat surfaces. Moreover, this hardness increases with increasing defect concentration. The same qualitative behaviour is

observed for sub-surface vacancies, although the effect is not as large as for self-interstitials.

From the results obtained by experiments and simulations we can conclude that the mechanical softening effect of surface defects associated with its roughness dominates over the hardening effect of sub-surface defects.

6. Conclusions

The main conclusion of the present work is that surface irregularities, deviating the position of the surface atoms from those of an ideal surface, always decrease the yield stress of a surface, the controlling mechanism being related to a lowering of the barriers required to nucleate dislocation loops at the surface. Previous work, reviewed here, had shown that multiple-stepped surfaces had a lower yield stress than low-index flat ones. In ion-irradiated surfaces, two competing mechanisms operate: one of increasing surface roughness—somehow equivalent to stepping the surface—and another one
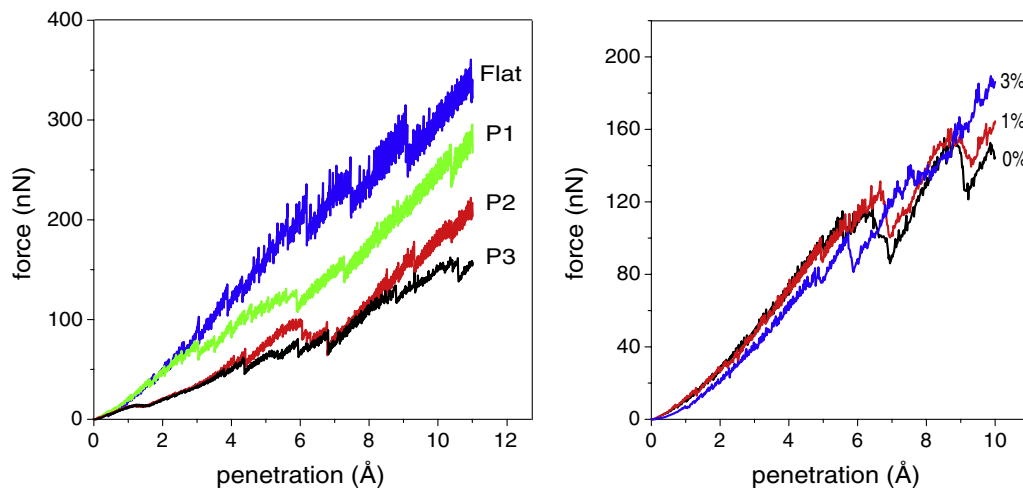
Figure 13. Simulated *F–h* curves of nanoindentation on (a) stepped pyramids (left) and (b) surfaces with interstitials placed below the surface (right). In the case of the pyramids, their inter-step distance decreases from P1 to P3 (and thus their steepnesses increase from P1 to P3). A nanoindentation curve on a flat surface is shown for comparison. For the case of the interstitials, two different defect concentrations are compared, again together with the case of the flat surface (with no defect concentration).

of increasing the concentration of defects at the surface and sub-surface level. Whereas the first one tends to soften the material, the second one tends to harden it and it is not obvious which one will prevail. We have shown that ion bombardment at high flux indeed reduces the onset of surface plasticity in ion-bombarded gold and, consequently, that the softening contribution of the roughening of the surface is dominating. Simulations of model systems involving surface defects confirm that trend.

Acknowledgments

References

[1] Haruta M 1997 *Catal. Today* **36** 153
[2] Meyer R, Lemire C, Shaikhutdinov Sh K and Freund H-J 2004 *Gold Bull.* **37** 72
[3] Fischer-Cripps A C 2004 *Nanoindentation* (New York: Springer)
[4] Gouldstone A, Chollacoop N, Dao M, Li J, Minor A M and Shen Y L 2007 *Acta Mater.* **55** 4015–39
[5] Christopher D, Smith R and Richter A 2001 *Nanotechnology* **12** 372
[6] Rodríguez de la Fuente O, Zimmerman J A, González M A, de la Figuera J, Hamilton J C, Pai W W and Rojo J M 2002 *Phys. Rev. Lett.* **88** 036101
[7] Smith R, Christopher D, Kenny S D, Richter A and Wolf B 2003 *Phys. Rev.* B **67** 245405
[8] Asenjo A, Jafaar M, Carrasco E and Rojo J M 2006 *Phys. Rev.* B **73** 075431
[9] Filleter T and Bennewitz R 2007 *Nanotechnology* **18** 044004
[10] Corcoran S G, Colton R J, Lilleodden E T and Gerberich W W 1997 *Phys. Rev.* B **55** R16057
[11] Zimmerman J A *et al* 2001 *Phys. Rev. Lett.* **87** 165507

[12] Navarro V, Rodriguez de la Fuente O, Mascaraque A and Rojo J M 2008 *Phys. Rev. Lett.* **100** 105504
[13] Valbusa U, Boragno C and Buatier de Mongeot F 2002 *J. Phys.: Condens. Matter* **14** 8153
[14] Chan W L and Chason E 2007 *Appl. Phys. Rev.* **101** 121301
[15] Makeev M A, Cuerno R and Barabasi A L 2002 *Nucl. Instrum. Methods* B **197** 185
[16] Rodríguez de la Fuente O, Borasio M, Galletto P, Rupprechter G and Freund H-J 2004 *Surf. Sci.* **566** 740
[17] Moroni R, Bisio F, de Mongeot F B, Canepa M, Boragno C, Mattera L and Valbusa U 2007 *Nucl. Instrum. Methods* B **257** 359
[18] Rodríguez de la Fuente O, González M A and Rojo J M 2001 *Phys. Rev.* B **63** 085420
[19] Nastasi M, Mayer J W and Hirvonen J K 1996 *Ion-Solid Interactions: Fundamentals and Applications* (Cambridge: Cambridge University Press)
[20] Girard J C, Samson Y, Gauthier S, Rousset S and Klein J 1994 *Surf. Sci.* **302** 73–80
[21] Ritter M, Stindtmann M, Farle M and Baberschke F 1996 *Surf. Sci.* **348** 243–52
[22] Busse C, Hansen H, Linke U and Michely T 2000 *Phys. Rev. Lett.* **85** 326
[23] González M A, de la Figuera J, Rodríguez de la Fuente O and Rojo J M 1999 *Surf. Sci.* **429** 486
[24] Rodríguez de la Fuente O, González M A and Rojo J M 2000 *Surf. Sci.* **454** 16
[25] Rodríguez de la Fuente O 2002 *Doctoral Thesis* Universidad Complutense Madrid
[26] Carrasco E, Rodríguez de la Fuente O, González M A and Rojo J M 2004 *Eur. Phys. J.* B **40** 421
[27] Constantini G, Rusponi S, Gianotti R, Boragno C and Valbusa U 1998 *Surf. Sci.* **416** 245–54
[28] El Gabaly F, Miranda R and de la Figuera J 2004 *Phys. Rev.* B **70** 012102
[29] Kittel C 1971 *Introduction to Solid State Physics* 3rd edn (New York: Wiley)
[30] Uchic M D, Dimiduk D M, Florando J N and Nix W D 2004 *Science* **67** 245405
[31] Durst K, Backes B, Franke O and Göken M 2006 *Acta Mater.* **54** 2547–55
[32] Butt H-J, Capella B and Kappl M 2005 *Surf. Sci. Rep.* **59** 1–152
[33] Li J 2007 *MRS Bull.* **32** 151

[34] Cross G L W, Schirmeisen A, Grütter P and Duerig U T 2006
      Nat. Mater. **5** 370
[35] Harvey S, Huang H, Venkataraman S and Gerberich W W 1993
      Acta Mater. **8** 1291
[36] Kracke B and Damaschke B 2000 *Appl. Phys. Lett.* **77** 361
[37] Kiely J D and Houston J E 1998 *Phys. Rev.* B **57** 12588
[38] Lim Y Y and Chaudry M M 1999 *Phil. Mag.* **79** 2979
[39] Schuh C A, Mason J K and Lund A C 2005 *Nat. Mater.* **4** 617
[40] Mason J K, Lund A C and Schuh C A 2006 *Phys. Rev.* B
      73 054102
[41] Kelchner C L, Plimpton S J and Hamilton J C 1998 *Phys. Rev.*
      B **58** 11085
[42] Zhu T *et al* 2004 *J. Mech. Phys. Solids* **52** 691
[43] Ferrando R, Andrei M, Relini A, Rolandi R and Gliozzi A 2005
      Phys. Rev. B **72** 045412
[44] Navarro V, Rodríguez de la Fuente O, Mascaraque A and
      Rojo J M 2008 *Phys. Rev.* B **78** 224107
[45] Johnson K L 1985 *Contact Mechanics* (Cambridge: Cambridge
      University Press)
[46] Johnson K L, Kendall K and Roberts A D 1971 *Proc. R. Soc.* A
      324 301
[47] Derjaguin B V, Muller V M and Toporov Y P 1975 *J. Colloid
      Interface Sci.* **53** 314
[48] Lorenz D, Zeckzer A, Hilpert U, Grau P, Johansen H and
      Leipner H S 2003 *Phys. Rev.* B **67** 172101
[49] Biener M M, Biener J, Hodge A M and Hamza A V 2007 *Phys.
      Rev.* B **76** 165422
[50] Knap J and Ortiz M 2003 *Phys. Rev. Lett.* **90** 226102
[51] Minor A M *et al* 2006 *Nat. Mater.* **5** 697
[52] Van Vliet K J, Li J, Zhu T, Yip S and Suresh S 2003 *Phys. Rev.*
      B **67** 104105
[53] Carrasco E, Rodríguez de la Fuente O, González M A and
      Rojo J M 2003 *Phys. Rev.* B **68** 180102
[54] Kiely J D, Hwang R Q and Houston J E 1998 *Phys. Rev. Lett.*
      81 4424
[55] Cannara R J, Bruckman M J and Carpick R W 2005 *Rev. Sci.
      Instrum.* **76** 053706
[56] Horcas I, Fernández R, Gómez-Rodríguez J M, Colchero J,
      Gómez-Herrero J and Baró A M 2007 *Rev. Sci. Instrum.*
      78 013705
[57] Oliver W C and Pharr G M 1992 *J. Mater. Res.* **7** 1564–83
[58] Foiles S M 1985 *Phys. Rev.* B **32** 3409–15
[59] Li J 2003 *Modelling Simul. Mater. Sci. Eng.* **11** 173
[60] Carrasco E, González M A, Rodríguez de la Fuente O and
      Rojo J M 2004 *Surf. Sci.* **572** 467
[61] Rodríguez de la Fuente O, González M A and Rojo J M 2003
      Phil. Mag. **83** 485
[62] Gannepalli A and Mallapragada S K 2002 *Nat. Mater.* **66**
      104103
[63] Jeng Y-R and Tan C-M 2004 *Phys. Rev.* B **69** 104109
[64] Hirth J P and Lothe J 1968 *Theory of Dislocations*
      (New York: McGraw-Hill)
[65] Yu H H *et al* 2007 *J. Mech. Phys. Solids* **55** 489